

Ultrafast Spin Dynamics in Ferromagnetic Nickel

E. Beaurepaire, J.-C. Merle, A. Daunois, and J.-Y. Bigot

*Institut de Physique et Chimie des Matériaux de Strasbourg, Unité Mixte 380046 CNRS-ULP-EHICS,
23, rue du Loess, 67037 Strasbourg Cedex, France*

(Received 17 October 1995)

The relaxation processes of electrons and spins systems following the absorption of femtosecond optical pulses in ferromagnetic nickel have been studied using optical and magneto-optical pump-probe techniques. The magnetization of the film drops rapidly during the first picosecond, but different electron and spin dynamics are observed for delays in the range 0–5 ps. The experimental results are adequately described by a model including three interacting reservoirs (electron, spin, and lattice). [S0031-9007(96)00167-6]

PACS numbers: 75.40.Gb, 75.70.-i, 78.20.Ls, 78.47.+p

Ultrafast optical spectroscopy is an ideal technique to investigate the electronic relaxation processes in metallic materials [1–3]. A femtosecond optical pulse can induce a nascent nonequilibrium electron gas which subsequently thermalizes to a Fermi distribution. This thermalization, which takes place within about 500 fs as measured for instance in noble metals, is due to electron-electron interactions [4–6]. In the next step, the hot electron gas relaxes its energy to the lattice due to electron-phonon interactions, a process which occurs within 1–10 ps depending on the incident laser intensity. During this time, the temperature exchange between the electron bath (temperature T_e) and the lattice (temperature T_l) can be investigated. From such measurements, one can deduce the characteristic times of the microscopic interactions which govern the basic metallic properties like electron transport and superconductivity [7].

In spite of the large amount of work performed in this field, little attention has been paid to magnetic effects occurring in the femtosecond time scale. An important challenge is to know whether the initial hot electron distribution can induce a spin dynamics associated with a spin temperature T_s different from T_e and T_l . This would lead to an ultrafast demagnetization, a relevant effect in regards to applications in magneto-optic devices. From a conceptual point of view, such a fast magnetization change is not trivial since the optical transitions preserve the electronic spin. However, one can expect that, during the transient hot electron regime, spin populations are modified due to spin dependent electron scattering. The characteristic time of this process has not been investigated with a femtosecond temporal resolution. Previous experiments performed with picosecond pulses on Ni [8] or Fe [9] have shown no demagnetization effect up to the melting point of the samples. The authors concluded that the spin-lattice relaxation times of these metals are larger than 30 ps. A more sophisticated pump-probe experiment, using 10 ns pump and 60 ps probe pulses, made on Gd films could deduce a spin-lattice relaxation time of 100 ± 80 ps [10,11]. All these experiments were performed on a time scale where

electrons and lattice temperatures are in equilibrium and therefore could not resolve separately the effects of electron-spin and spin-lattice relaxation mechanisms on the demagnetization process.

The aim of this paper is to study both electronic and spin dynamics after excitation of a Ni film with 60 fs pulses. Using two independent pump-probe measurements (optical and magneto-optical), the dynamics of both the electronic and spin temperatures are obtained. It is shown that during the relaxation of electrons to the lattice, the spin temperature T_s can be increased up to ~ 575 K within 2 ps for pulses of 7 mJ cm^{-2} . To our knowledge, this temporal behavior is much faster than any spin dynamics reported until now in a metallic ferromagnet. In addition, a phenomenological model based on the interactions between three baths (electrons, spins, and phonons) is developed, and accounts well for the observed dynamics.

In the present work, we have studied ferromagnetic Ni since its Curie temperature (631 K) is the lowest among 3d transition metals. Polycrystalline thin films of 22 nm thickness are prepared by thermal evaporation in high vacuum. They are protected by a 100 nm MgF_2 coating. The thicknesses of the Ni and MgF_2 layers are determined by grazing incidence x-ray reflectivity. An atomic force microscopy characterization performed on uncoated films shows a surface roughness of about 2 nm and structures with lateral dimensions of the order of 20 nm, which we attribute to crystalline domains. Two types of dynamical measurements have been made. The spin dynamics has been measured in the time resolved magneto-optical Kerr effect (MOKE) configuration. As shown in Fig. 1(a), the longitudinal MOKE signal is measured with p -polarized light incident at 45° on the sample (located in the gap of a 3 kOe electromagnet) by detecting the intensity of the reflected beam with a nearly crossed analyzer. As displayed in Fig. 1(b), for each delay Δt between the pump and probe pulses, a full hysteresis loop is recorded. The second type of measurement consists of pump-probe transmission experiments without magnetic field. It allows us to study the electronic thermalization process and to deduce the electronic temperature T_e . A typical

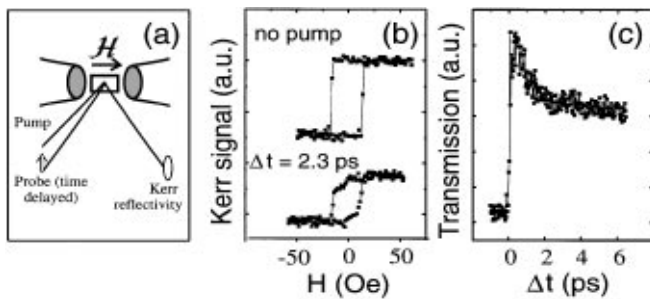


FIG. 1. (a) Experimental pump-probe setup allowing dynamic longitudinal Kerr effect and transient transmissivity or reflectivity measurements. (b) Typical Kerr loops obtained on a 22 nm thick Ni sample in the absence of pump beam and for a delay $\Delta t = 2.3$ ps between the pump and probe pulses. The pump fluence is 7 mJ cm^{-2} . (c) Transient transmissivity [same experimental condition as (b)].

transient transmission curve $\Delta T/T$ is displayed in Fig. 1(c). For both techniques, we used 60 fs pulses coming from a 620 nm colliding pulse mode locked dye laser and amplified by a 5 kHz copper vapor laser. The temporal delays between pump and probe are achieved using a modified Michelson interferometer. The signals are recorded using a boxcar and a lock-in synchronous detection. In the case of differential transmission measurements, the synchronization is made by chopping the pump beam, while for the MOKE measurements it is done on the probe beam.

The information about the spin dynamics is contained in the time evolution of the hysteresis loops recorded for each time delay Δt . Typical loops obtained for $\Delta t = 2.3$ ps and in the absence of the pump beam are presented in Fig. 1(b). Each hysteresis loop is recorded at a fixed delay by slowly sweeping the magnetic field H . For each H value, the MOKE signal is averaged over about 100 pulses. The most striking feature is an important decrease of the remanence (signal at zero field) M_r when the pump is on. The complete dynamics $M_r(\Delta t)$ for a laser fluence of 7 mJ cm^{-2} is displayed in Fig. 2. The overall behavior is an important and rapid decrease of M_r which occurs within 2 ps, followed by a relaxation to a long lived plateau. This figure clearly shows that the magnetization of the film drops during the first picosecond, indicating a fast increase of the spin temperature. It can be noticed that for negative delays M_r does not completely recover its value measured in the absence of pump beam. This permanent effect is not due to a sample damage as checked by recording hysteresis loops without the pump beam after the dynamical measurements. Possible explanations for this small permanent change are either heat accumulation or slow motion of the domain walls induced by the pump beam.

In order to determine the temperature dynamics, we analyze Fig. 2 using the static temperature dependence of the magnetization found in text books. This analysis relies on a correspondence between the variations of the

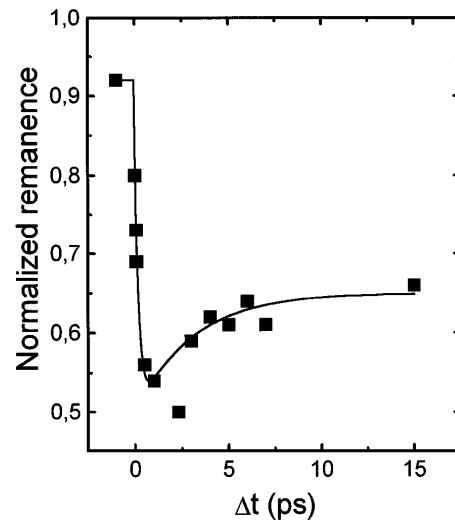


FIG. 2. Transient remanent longitudinal MOKE signal of a Ni(20 nm)/MgF₂(100 nm) film for 7 mJ cm^{-2} pump fluence. The signal is normalized to the signal measured in the absence of pump beam. The line is a guide to the eye.

spontaneous and remanent magnetization, as is usually done in thin film magnetism. This leads to the time variation of T_s in Fig. 3(a) (dotted points). Regarding the determination of the electronic temperature, we assume that it is proportional to the differential transmittance shown in Fig. 1(c) as expected for weak $\Delta T/T$ signals. Let us emphasize that this procedure is valid only when a thermalized electron population can be defined. Since this effect was never discussed for the case of d electrons in metals, it deserves some comments. As discussed by various authors [4–6], the optical pulse creates in the metal film a nascent (nonthermal) electronic distribution that relaxes due to electron-electron interactions, leading to a fast increase of the electron temperature. This process can be described in the random phase approximation (RPA) defining nonthermal and thermal (in the sense of the Fermi-Dirac statistics) electron populations. The nonthermal electron population is therefore created during the pump pulse and disappears with a characteristic time τ_{th} (≈ 500 fs for Au), whereas the temperature of the thermal population increases in the same time scale. The contribution of the nonthermal electronic distribution to the transient optical data is therefore expected to present a sharp peak around zero probe delay (with a rise time given by the temporal resolution) and the thermal electron contribution should present a delayed extremum around τ_{th} [5]. A detailed analysis of the transient effects in Ni for short delays is beyond the scope of the present paper and will be presented in a future publication. Let us only mention that with the present experimental conditions the transient reflectivity of the Ni film presents a single contribution which is extremum for $\Delta t = 260$ fs showing that the contribution of nonthermal populations is weak and that the thermalization time is $\tau_{\text{th}} \approx 260$ fs. This short thermalization time for Ni as compared to Au is

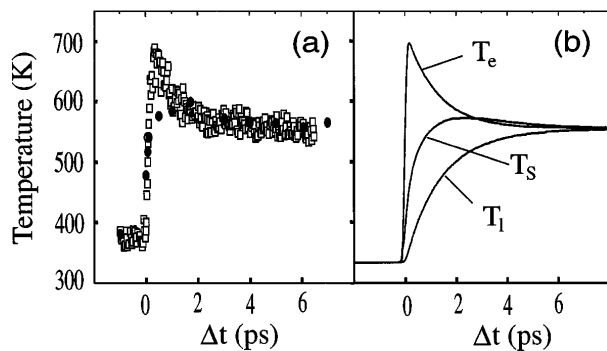


FIG. 3. (a) Experimental spin (T_s) and electron (T_e) temperatures estimated as explained in the text. The experimental conditions are those of Fig. 2. (b) Calculated spin (T_s), electron (T_e), and lattice (T_l) temperatures from Eqs. (1). The relevant parameters are given in the text.

qualitatively explained by the flatness of $3d$ bands (in the RPA, τ_{th} scale as E_F^2) and the effects of electron correlations that are known to reduce the lifetime of excited electronic states [12–14]. This estimation of τ_{th} allows us to set a lower limit where a model with thermalized baths, as used later on, is valid.

The temperature variation of T_e deduced from differential transmittance is plotted in Fig. 3(a) (squares), where the absolute electronic temperature scale is obtained by normalization to T_s at negative and large positive delays ($\Delta t > 10$ ps). On this time scale, the electron temperature presents a sharp peak up to $T_e = 675$ K and then an exponential-like decay with a characteristic time of the order of 1 ps until a saturation at $T_e = 550$ K is reached. On the other hand, the spin temperature rises rapidly during the first picosecond, presents a broad maximum $T_s = 580$ K around 2 ps, and then, for longer delays, follows the same trend as the electron temperature. Therefore, the peak observed for the electron temperature has a delayed and smoothed counterpart in the spin temperature. This delay can be qualitatively understood remembering that, within the dipole approximation, the optical transitions preserve the electronic spins, such that the spin polarization of the nascent electronic distribution is the same as in the ground state. After a finite time, scattering takes place and the majority and minority spins tend to homogenize, leading to an increase of T_s . As discussed below, a simple model helps to understand the role of the different types of interaction processes.

The preceding effects can be accounted for by using a phenomenological description which extends the modelization of electron thermalization in metals (the so-called two temperatures model [15]) to spin effects. We assume the existence of three thermalized reservoirs that exchange energy, namely, the electron system at temperature T_e , the spin system at temperature T_s , and the lattice or phonons at temperature T_l . The temporal evolution of the system is described by the three coupled differential equations:

$$\begin{aligned}
 C_e(T_e)dT_e/dt &= -G_{el}(T_e - T_l) \\
 &\quad - G_{es}(T_e - T_s) + P(t), \\
 C_s(T_s)dT_s/dt &= -G_{es}(T_s - T_e) - G_{sl}(T_s - T_l), \\
 C_l(T_l)dT_l/dt &= -G_{el}(T_l - T_e) - G_{sl}(T_l - T_s),
 \end{aligned} \tag{1}$$

where C_e is the electronic specific heat of Ni. C_s (C_l) is the magnetic (lattice) contribution to the specific heat. G_{el} , G_{es} , and G_{sl} are the electron-lattice, electron-spin, and spin-lattice interaction constants. They are taken as free parameters that allow one to describe the energy transfer rate from the electron system to the spin and the lattice. The laser source term $P(t)$ in Eqs. (1) is applied only to the electronic terms since the initial heating process occurs only in the electron bath. In the present study, we assume uniform temperature profiles and, therefore, neglect heat propagation. Indeed, transverse heat propagation is negligible on the picosecond time scale over the beam spot diameter ($\sim 30 \mu\text{m}$). In addition, longitudinal temperature gradients are neglected due to the small sample thickness.

The set of Eqs. (1) has been solved numerically using a fifth order predictor-corrector Adam method, using Gaussian pulses of 100 fs duration. As seen in Fig. 3(b), the simulated temperature dynamics are in good agreement with the observed behavior.

In the numerical calculation, we assume that C_l is independent of the lattice temperature and given by $C_l = C(300 \text{ K}) - C_e(300 \text{ K}) = 2.2 \times 10^6 \text{ J m}^{-3} \text{ K}^{-1}$, where $C(300 \text{ K}) = 4 \times 10^6 \text{ J m}^{-3} \text{ K}^{-1}$ is the experimental total specific heat of Ni [16]. This approximation is valid since the experiment is performed at room temperature and therefore $T_l \geq \Theta_D$, Θ_D being the Debye temperature (475 K for Ni [17]). We checked that in the temperature range involved C_l as given by the Debye theory is constant within 5%. The electronic specific heat C_e is taken proportional to the temperature: $C_e = \gamma T_e$. In the present simulation we used an effective $\gamma = 6 \times 10^3 \text{ J m}^{-3} \text{ K}^{-2}$ which is larger than the value obtained at low temperature [18]. This discrepancy can be attributed to the fact that the density of states possesses strong singularities around the Fermi level [19]. These singularities which have little influence at low temperatures (typically $T_e \leq 10$ K) become predominant in the temperature range $295 < T_e < 700$ K explored in the first few hundred femtoseconds. It may also be due to the fact that nonthermal electron populations are not considered in Eqs. (1). C_s represents the spin specific heat which is maximum at the Curie temperature ($T_C = 631$ K). The variation of C_s with T_s is obtained from the total specific heat C by subtracting the linear contribution coming from the lattice and the electrons.

We now describe the influence of the free parameters on the solutions. It is found that the value of $P(t)$ is essential for the determination of T_e maximum and was adjusted to reproduce the experimental value of Fig. 3(a). This

value is consistent with previous work on Cu films with the same experimental setup and also with an estimation of the pump fluence. As expected, G_{el} mainly determines the decay of the electronic temperature until equilibrium is reached, whereas G_{es} qualitatively sets the maximum value of T_s and G_{sl} the delay when this maximum occurs. Figure 3(b) shows that the salient features in the experimental variations of T_e and T_s are fairly well reproduced by a simulation with $G_{el} = 8 \times 10^{17} \text{ W m}^{-3} \text{ K}^{-1}$, $G_{es} = 6 \times 10^{17} \text{ W m}^{-3} \text{ K}^{-1}$, and $G_{sl} = 0.3 \times 10^{17} \text{ W m}^{-3} \text{ K}^{-1}$. In opposition to previous interpretations of experiments in the subnanosecond time scale [10,11,20], we find that in the picosecond regime the main interactions are the electron-lattice and electron-spin type, the electron-electron interactions occurring on a shorter time scale [4]. The present results clearly establish that ultrafast heating of the spin population can be induced via the G_{es} coupling constant. The above phenomenological model allows us to reproduce the electron and spin dynamics on a picosecond range. However, an accurate description of the behavior at short delays would require a more sophisticated model describing the dynamics of a nonthermal (in the sense of Fermi-Dirac statistics) spin polarized electron gas. An extension of the model developed by Sun and co-workers [5], which includes nonthermal electron populations, shows that the estimations of interaction constants are not strongly affected by the presence of the nonthermal population for short delays.

The preceding observations are of great potential consequences for magneto-optical applications since a fast demagnetization can be induced optically. However, it can be noticed that the Curie temperature has not been reached in the experiment, so that a complete ferroparamagnetic transition was not achieved. Increasing the laser fluence by a factor of 2 leads to an irreversible sample damage. This damage manifests by a decrease of the contrast in the hysteresis loops $M(H)$. It does not affect the transmission of the sample, and we observed unmodified differential transmission curves $\Delta T/T$ for these highest fluences. We attribute these effects to a permanent rearrangement of sample domains without a major crystallographic alteration by the pump pulses. These observations suggest that an appropriate monitoring of the material properties should be made to obtain efficient devices that can operate above the Curie temperature. In order to evaluate the adequate material characteristics we used the above model to predict the dynamical behavior. Two types of behaviors are interesting with respect to applications. First, a transient ultrafast demagnetization might be desirable for device operations. The present study indicates that this process can occur in the picosecond or subpicosecond time scale, although it was not completely achieved in the experiment since the maximum spin temperature stayed slightly below T_c . Another interesting situation is to induce a permanent switch of the magnetization direction. This effect would require low T_c materials as well as a low electronic specific heat.

In conclusion, by combining optical and magneto-optical measurement techniques, we have reported experimental results in metallic nickel films showing that a fast subpicosecond demagnetization can be induced using femtosecond optical pulses. The measurements allow us to deduce the electron and spin temperatures T_e and T_s and show that, during the first few picoseconds, their dynamics are different. A phenomenological model describing the heat transfer between three coupled baths (electrons, spins, and lattice) is presented. It allows us to give a value for the electron-spin coupling constant G_{es} , a parameter which so far was not investigated in ferromagnets. The present study is important for the fundamental understanding of the dynamics of electron-spin interactions. In addition, it is a major step towards the determination of the limitations of dynamical magneto-optical materials since it indicates that a subpicosecond demagnetization may occur in appropriately designed devices.

This work is partly supported by the ULTIMATECH program of the C.N.R.S. We thank G. Versini for sample preparation, M. Robino for AFM characterization, C. Ulhac for x-ray diffraction on the samples, and G. Garreau for participation in a preliminary experiment.

-
- [1] G. L. Eesley, Phys. Rev. Lett. **51**, 2140 (1983).
 - [2] H. E. Elsayed-Ali *et al.*, Phys. Rev. Lett. **58**, 1212 (1987).
 - [3] R. W. Schoenlein *et al.*, Phys. Rev. Lett. **58**, 1680 (1987).
 - [4] W. S. Fann *et al.*, Phys. Rev. B **46**, 13 592 (1992).
 - [5] C. K. Sun *et al.*, Phys. Rev. B **50**, 15 337 (1994).
 - [6] C. Suarez, W. E. Bron, and T. Juhasz, Phys. Rev. Lett. **75**, 4536 (1995).
 - [7] S. D. Brorson *et al.*, Phys. Rev. Lett. **64**, 2172 (1990).
 - [8] M. B. Agranat *et al.*, Zh. Eksp. Teor. Fiz. **86**, 1376 (1984) [Sov. Phys. JETP **59**, 804 (1984)].
 - [9] A. Vaterlaus *et al.*, J. Appl. Phys. **67**, 5661 (1990).
 - [10] A. Vaterlaus, T. Beutler, and F. Meier, Phys. Rev. Lett. **67**, 3314 (1991).
 - [11] A. Vaterlaus *et al.*, Phys. Rev. B **46**, 5280 (1992).
 - [12] D. Chandesris, Thèse d'Etat, Université de Paris Sud, 1983.
 - [13] A. Liebsch, Phys. Rev. Lett. **43**, 1431 (1979).
 - [14] G. Treglia, F. Ducastelle, and D. Spanjaard, J. Phys. (Paris) **43**, 341 (1982).
 - [15] S. I. Anisimov, B. L. Kapeliovitch, and T. L. Perel'man, Zh. Eksp. Teor. Fis. **66**, 776 (1974) [Sov. Phys. JETP **39**, 375 (1974)].
 - [16] E. Lapp, Ann. Phys. (Paris) **XII**, 442 (1929); see also M. Braun, R. Kohlhaas, and O. Vollmer, Z. Angew. Phys. **25**, 365 (1968).
 - [17] M. Dixon *et al.*, Proc. R. Soc. London A **285**, 561 (1965).
 - [18] C. Kittel, *Introduction to Solid State Physics* (John Wiley and Sons, New York, 1976), p. 167.
 - [19] V. L. Moruzzi, J. F. Janak, and A. R. Williams, *Calculated Electronics Properties of Metals* (Pergamon Press, New York, 1978), p. 182.
 - [20] L. Callegaro and E. Puppini, Phys. Status Solidi (b) **185**, 481 (1994).